



Cite this: Mater. Adv., 2022,
3, 3593

Received 19th January 2022,
Accepted 6th March 2022

DOI: 10.1039/d2ma00058j

rsc.li/materials-advances

MoS₂ nanosheets for the detoxification of Hg²⁺ in living cells[†]

Shanshan Xing, Chunqiu Xia, Xinyi Liu, Liangqia Guo * and Fengfu Fu 

A simple and green one-step method for the simultaneous exfoliation and functionalization of few-layered MoS₂ nanosheets was developed *via* the ultrasonic treatment of bulk MoS₂ powder in sodium phytate-containing aqueous solution. The as-prepared MoS₂ nanosheets show high stability, low cytotoxicity and high adsorption capacity for Hg²⁺ in aqueous solution. The maximum adsorption capacity for Hg²⁺ is about 7.5 times and 3.7 times that of bulk MoS₂ powder and unfunctionalized MoS₂ nanosheets, respectively. The adsorption kinetics and thermodynamics indicate that the adsorption of Hg²⁺ is a monolayer chemical adsorption. Finally, the as-prepared MoS₂ nanosheets were applied for the removal of Hg²⁺ in HepG2 cells and show a similar detoxification effect as that of the common antidote *meso*-2,3-dimercaptosuccinic acid, indicating the potential application of MoS₂ nanosheets for biological detoxification.

1. Introduction

The mercury ion (Hg²⁺) is a highly toxic ion that can cause gastrointestinal mucosal and kidney failure, central nervous system damage and even death.^{1,2} Hg²⁺ contamination has become increasingly serious in our living environment and ecosystem. The development of efficient technologies for the removal of Hg²⁺ has received tremendous attention. Traditional Hg²⁺ removal technologies include chemical precipitation,³ electrochemical processes,⁴ adsorption,⁵ membrane separation,⁶ ion exchange⁷ and solvent extraction.⁸ Among these technologies, adsorption has the advantages of simple operation and low cost. Owing to the large number of sulfur (S) atoms exposed on the surface and the strong soft-soft interaction between Hg²⁺ and S, molybdenum disulfide (MoS₂), a typical layered transition-metal dichalcogenide (TMDC)⁹ composed of a hexagonal plane with Mo atoms sandwiched by two sulfur atoms (S-Mo-S), can be used as a promising adsorbent for the removal of Hg²⁺.¹⁰ Therefore, MoS₂ nanosheets with widened interlayer spacing,¹⁰ two-dimensional (2D) MoS₂ nanosheets,¹¹

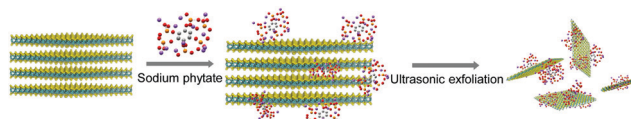
oxygen-incorporated MoS₂ nanosheets,¹² Au/Fe₃O₄/MoS₂ aerogels,¹³ d-MoS₂/Fe₃O₄ nanohybrids,¹⁴ and cellulose/MoS₂/Fe₃O₄ composites¹⁵ have been shown to be excellent adsorbents for the removal of Hg²⁺ from aqueous solutions. Although these MoS₂-based adsorbents show high adsorption capacity for Hg²⁺, they are still in the proof-of-concept phase and none of the MoS₂-based adsorbents have been applied to remove Hg²⁺ in real complex environmental and biological samples.

Bulk MoS₂ has strong chemical bonding within its layers and weak van der Waals forces between its layers. To expose more surfaces with S atoms to the outside for adsorption, the exfoliation of bulk MoS₂ into single- or few-layered nanosheets is necessary. To date, chemical exfoliation with alkali metal compounds and liquid-phase exfoliation are recognized as effective methods for the scale-up production of MoS₂ nanosheets.¹⁶ However, chemical exfoliation requires a harsh and strong intercalating reagent (such as *n*-butyl lithium) followed by ultrasonic exfoliation under inert atmosphere.^{17,18} Moreover, the preparation procedure is expensive, dangerous, long and tedious. Liquid-phase exfoliation of bulk MoS₂ *via* facile ultrasonic treatment in organic solvents, such as ethanol,^{19,20} 2-propanol,²¹ *N*-methyl-2-pyrrolidone,²² acetone and alcohols (ethanol, methanol and isopropanol),²³ or in aqueous solution with auxiliary reagents such as thiolated surfactants,²⁴ polystyrene-polyacrylamide,²⁵ bovine serum albumin,²⁶ poly(3,4-ethylenedioxothiophene):poly-(styrenesulfonate),²⁷ Nafion,²⁸ and polymeric ionic liquids,²⁹ has been successfully developed and is widely applied in the fields of catalysis, organic solar cells, antibacterial materials, conductive films, *etc.* However, these organic solvents, surfactants, and polymers are mostly toxic, and will thus cause adverse effects in biological applications. Therefore, a facile method for the

Ministry of Education Key Laboratory for Analytical Science of Food Safety and Biology, Fujian Provincial Key Laboratory of Analysis and Detection Technology for Food Safety, College of Chemistry, Fuzhou University, Fuzhou 350116, China.
E-mail: lqguo@fzu.edu.cn

[†] Electronic supplementary information (ESI) available: Adsorption spectra of MoS₂ nanosheets at different conditions, XRD pattern, Raman spectra, adsorption spectra of MoS₂ nanosheets with different reagents, effect of pH on the adsorption amount, Langmuir adsorption isotherms, XPS spectra of MoS₂ nanosheets, adsorption selectivity, viability of HepG2 cells, comparison of yields of MoS₂ nanosheets, adsorption dynamics model parameters, the maximal adsorption capacity and correlation coefficient of Langmuir isotherms, comparison of the maximum adsorption capacity of MoS₂ for Hg²⁺. See DOI: 10.1039/d2ma00058j





Scheme 1 Schematic illustration of the exfoliation of bulk MoS_2 and the functionalization of MoS_2 nanosheets by phytate.

exfoliation and functionalization of MoS_2 nanosheets with a green and cost-effective auxiliary reagent to reinforce their biocompatibility and functionality for biological application is highly desired.^{30,31}

Herein, we report a facile green method to simultaneously exfoliate and functionalize MoS_2 nanosheets *via* ultrasonic treatment of bulk MoS_2 in sodium phytate-containing aqueous solution (Scheme 1). Sodium phytate is the sodium salt of phytic acid (myo-inositol-1,2,3,4,5,6-hexakisphosphate) extracted from rice bran and is a natural chelating agent. The as-prepared MoS_2 nanosheets show high stability in phosphate buffer solution in the pH range of 2.0–12.0 and low cytotoxicity. Taking advantage of the high binding affinity between Hg^{2+} and S sites on the surface of MoS_2 sheets^{10,11} and the biocompatible, biodegradable, and nontoxic phytate,³² the as-prepared MoS_2 nanosheets were used as an adsorbent for the removal of Hg^{2+} from water and as a detoxifier for the removal of Hg^{2+} in HepG2 cells. Our results indicate that the as-prepared MoS_2 nanosheets display a detoxification effect that is comparable to that of *meso*-2,3-dimercaptosuccinic acid (DMSA), a heavy metal detoxifier approved by the Food and Drug Administration of USA for the treatment of lead and mercury toxicity both in children and adults. To the best of our knowledge, this work is the first example to use TMDC for heavy metal detoxification in living cells.

2. Experimental

2.1. Chemical and materials

Bulk MoS_2 powder and DMSA were purchased from Shanghai Aladdin Biochemical Technology. Sodium phytate was bought from Sangon Biotech (Shanghai) Co., Ltd. Hg^{2+} standard solution ($1000 \mu\text{g mL}^{-1}$) in 1.0 mol L^{-1} HNO_3 was obtained from the National Nonferrous Metals and Electronic Materials Analysis and Testing Center of China, and was diluted to the desired concentration with water. Dulbecco's modified Eagle's medium (DMEM), phosphate buffered solution (PBS, 10 mmol L^{-1} , pH 7.4) and Cell Counting Kit-8 (CCK-8) were purchased from GE Healthcare Life Sciences HyClone laboratories, Inc. Without specification, the metal ions were nitrate salts and anions were sodium salts. All water used was ultrapure water ($18.2 \text{ M}\Omega \text{ cm}$, Millipore).

2.2. Exfoliation and functionalization of MoS_2 nanosheets by phytate

200 mg Bulk MoS_2 powder was added to 40 mL aqueous solution containing 40 mg sodium phytate. The suspension was ultrasonically treated for 35 h. The dispersion was centrifuged at 5000 rpm for 20 min to remove large particles, and the supernatant was further centrifuged at 12 000 rpm for 10 min to

remove excessive sodium phytate. The precipitate was collected and redispersed in water. The removal of sodium phytate in the supernatant was repeated three times, and the collected precipitate was redispersed in water for further use. In addition, bulk MoS_2 powder was separately exfoliated in Na_2HPO_4 solution and water under the same conditions.

2.3. Adsorption of Hg^{2+} by MoS_2 nanosheets

MoS_2 nanosheets exfoliated by sodium phytate (6.4 mg) were added to 30 mL Hg^{2+} solution with different concentrations (100 ng mL^{-1} , $1 \mu\text{g mL}^{-1}$, $10 \mu\text{g mL}^{-1}$ and $20 \mu\text{g mL}^{-1}$). The mixture solution was shaken at a rate of 300 rpm at room temperature (25 °C). An aliquot of 2 mL mixture solution was taken out at a certain time interval. After centrifugation at 12 000 rpm for 20 min, the supernatant was collected and filtered by a 0.22 μm filter to remove large particles. The concentration of residual Hg^{2+} in the filtrate was determined by ICP-MS.

2.4. Cytotoxicity assay and detoxification experiment

For the cytotoxicity assay, human hepatoma cells (HepG2) were treated with 0.25% trypsin for 1 min. After the trypsin solution was discarded, HepG2 cells were dispersed in DMEM medium by blowing. Then, HepG2 cells (1×10^5 cell in each well) were plated in a 96-microwell microplate and cultured in DMEM at 37 °C in a humidified 5% CO_2 incubator for 24 h. After the cells were washed with PBS (10 mmol L^{-1} , pH 7.4) three times to remove the secretions and culture medium, 100 μL MoS_2 nanosheets exfoliated by sodium phytate (0, 50, 100, 250, 500 and $1000 \mu\text{g mL}^{-1}$), Hg^{2+} (0, 0.5, 1, 2, 5 and $10 \mu\text{g mL}^{-1}$), or DMSA (0, 50, 100, 150 and $200 \mu\text{g mL}^{-1}$) in DMEM were each added and cultured at 37 °C in a humidified 5% CO_2 incubator for 12 h. After being washed with PBS (10 mmol L^{-1} , pH 7.4) three times, 10 μL CCK-8 and 90 μL DMEM were added to each well and the cells were incubated in the dark for 2 h. Finally, the absorbance of each well at 450 nm was recorded. Each experiment was repeated five times. The relative survival rate of the cells was calculated by taking the cell survival rate of the blank as 100%.

To investigate the detoxification effect of the MoS_2 nanosheets exfoliated by sodium phytate, 100 μL Hg^{2+} ($2 \mu\text{g mL}^{-1}$) in DMEM was added to HepG2 cells (1×10^5 cell) and incubated in the dark for 2 h. After the cells were washed with PBS (10 mmol L^{-1} , pH 7.4) three times, 11 μL MoS_2 nanosheets or DMSA in DMEM (0, 50, 100, 150 and $200 \mu\text{g mL}^{-1}$) was further added. After further incubation for 12 h, the cells were washed with PBS (10 mmol L^{-1} , pH 7.4) three times. The CCK-8 assay was used to detect the relative survival rate of the cells. Each experiment was repeated five times.

3. Results and discussion

3.1. Optimization of the exfoliation conditions

Bulk MoS_2 powder was ultrasonically exfoliated in sodium phytate aqueous solution. The exfoliation conditions (such as ultrasonication time, concentrations of sodium phytate and bulk MoS_2 powder) were optimized. The absorbance of the



MoS₂ nanosheets gradually increased with increasing time, and reached the platform until the ultrasonic time was up to 35 h (Fig. S1A, ESI†). The exfoliation yield, namely the mass ratio of the collected MoS₂ nanosheets to bulk MoS₂ powder, was increased with the concentration of sodium phytate until its concentration reached 1 mg mL⁻¹ (Fig. S1B, ESI†). However, when the concentration of sodium phytate exceeded 1 mg mL⁻¹, the exfoliation yield was decreased. Similarly, the exfoliation yield was increased with the concentration of bulk MoS₂ powder until its concentration reached 8 mg mL⁻¹ (Fig. S1C, ESI†). The exfoliation yield was reduced instead with the further increase of bulk MoS₂ powder. Therefore, the optimal conditions for the exfoliation of MoS₂ nanosheets are 35 h ultrasonic time, 1 mg mL⁻¹ sodium phytate and 8 mg mL⁻¹ bulk MoS₂ powder. Under the optimal conditions, the exfoliation yield is 18.1%, which is 8 times that of the MoS₂ nanosheets exfoliated in pure water. As shown in Table S1 (ESI†), the ultrasonic exfoliation yield is also higher than those by ultrasonic exfoliation in most solvents. The effect of pH on the stability of MoS₂ nanosheets was also investigated (Fig. S1D, ESI†). MoS₂ nanosheets can be dispersed stably in phosphate buffer (10 mmol L⁻¹) over a pH range of 2.0–12.0, indicating that the functionalization of phytate on the surface of the MoS₂ nanosheets endows their high stability in aqueous solution.

3.2. Characterization of MoS₂ nanosheets

There are two distinctive absorption peaks at 665 nm and 603 nm (A and B excitons, respectively) in the absorption spectrum of the MoS₂ nanosheets solution (Fig. 1A), which are typical characteristics of the hexagonal symmetry space group of 2H-MoS₂, corresponding to the direct excitonic transition of MoS₂ at the *K*-points of the Brillouin zone.^{23,28} According to the relationship between the mean number of layers and the wavelength of the A-exciton (λ_A) proposed by Coleman and co-workers,³¹ the mean number of layers is estimated to be less than 3. The potential of MoS₂ nanosheets was measured to be -33.4 mV (Fig. 1B), indicating that the functionalization by

phytate endows the MoS₂ nanosheets with abundant negative charges and high hydrophilicity and dispersity in aqueous solution. Moreover, the MoS₂ nanosheets show monodispersity with the most probable size of about 90 nm (Fig. 1C).

As observed from the low-resolution TEM image (Fig. 1D), MoS₂ nanosheets are composed of sheet-like structures from monolayers to few layers with lateral sizes from several dozens to a few hundreds of nanometers. The ordered lattice and parallel fringe can be clearly observed in the high-resolution TEM (HRTEM) image (Fig. 1E). The lattice spacing of 0.27 nm is indexed to the (100) plane of MoS₂.^{10,27,30} The selected area electron diffraction (SAED) pattern (inset of Fig. 1E) further confirms the single crystalline nature of the hexagonal symmetry structure of MoS₂ nanosheets. The thickness of the MoS₂ nanosheets is less than 2 nm, which is observed from the AFM image (Fig. 1F). According to the Bragg equation, the interlayer distance of the MoS₂ nanosheets was calculated to be 0.62 nm.^{23,33} Therefore, the layer number is about 2 to 3, which is in agreement with the result from the absorption spectrum.

As shown in the XRD patterns (Fig. S2A, ESI†), MoS₂ nanosheets maintain high crystallinity as bulk MoS₂ powder, indicating that there is no phase conversion during ultrasonic exfoliation. The diffraction peaks at 14.4°, 32.7°, 39.6°, 44.3°, 49.8°, 58.3° and 60.4° correspond to the (002), (100), (103), (006), (105), (110) and (008) crystal faces of 2H-MoS₂ (JCPDS No. 24-0513), respectively. The relative intensity of the (002) peaks in the MoS₂ nanosheets exfoliated by sodium phytate is weaker than bulk MoS₂ powder, indicating the successful exfoliation of the MoS₂ nanosheets.³⁴ Raman spectra (Fig. S2B, ESI†) show the characteristic in-plane (E_{2g}¹) and out-of-plane (A_{1g}) vibrational modes of MoS₂ at about 380 cm⁻¹ and 405 cm⁻¹.^{11,23} Compared with bulk MoS₂ powder, the vibration modes of MoS₂ nanosheets are red-shifted due to the weakening of the van der Waals force between the layers,³⁵ which also suggests the successful exfoliation of bulk MoS₂ into few-layered nanosheets.³⁶ There is also a rather weak second-order scattering process near 450 cm⁻¹, attributed to the longitudinal acoustic vibrational mode of the 2H phase monolayer MoS₂ nanosheets.³⁷

The survey XPS spectrum (Fig. 2A) indicates there are Mo, S, P, C and O elements in the MoS₂ nanosheets exfoliated by phytate, indicating that phytate is functionalized on the surface of the MoS₂ nanosheets. In the Mo 3d core-level XPS spectrum of MoS₂ nanosheets exfoliated by sodium phytate (Fig. 2B), the peaks at 229.3 eV and 232.5 eV can be attributed to Mo⁴⁺ 3d_{5/2} and Mo⁴⁺ 3d_{3/2} of 2H-MoS₂. The weak peaks at 235.7 eV and 233.0 eV can be ascribed to Mo⁶⁺ 3d_{3/2} and Mo⁶⁺ 3d_{5/2}, respectively. This also can be observed in the Mo 3d core-level XPS spectra of the MoS₂ nanosheets exfoliated by H₂O and bulk MoS₂ powder, and may come from MoO₃ or MoO₄²⁻,^{23,30} indicating that the surface of the MoS₂ nanosheets is partially oxidized on exposure to air.^{23,38} The weak feature peak at 226.6 eV originated from the S 2s.³⁹ In the S 2p core-level XPS spectrum (Fig. 2C), the peaks at 162.2 eV and 163.4 eV can be attributed to S 2p_{3/2} and S 2p_{1/2}, respectively. In addition, there exists a weak peak at 133.8 eV (Fig. 2D), corresponding to the

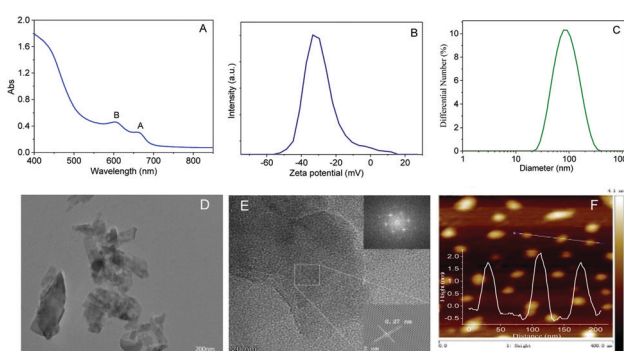


Fig. 1 (A) Absorption spectrum, (B) zeta potential distribution, (C) size distribution, (D) TEM image, (E) HRTEM and (F) AFM images of MoS₂ nanosheets exfoliated by sodium phytate. Insets of (E) and (F) are the SAED pattern and the height profile of MoS₂ nanosheets exfoliated by sodium phytate, respectively. The concentration of MoS₂ nanosheets in (A) is 1.12 mg mL⁻¹.



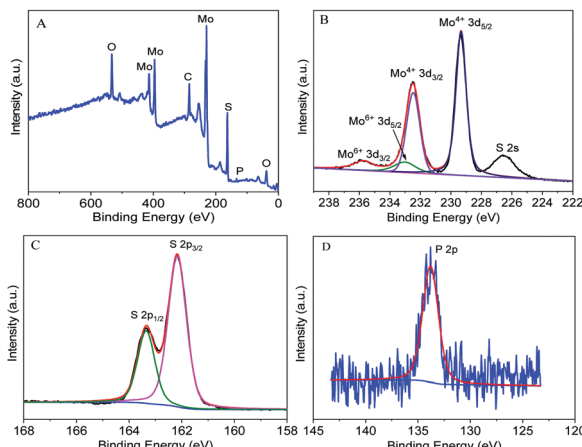


Fig. 2 The survey (A), Mo 3d (B), S 2p (C) and P 2p (D) core-level XPS spectra of MoS₂ nanosheets exfoliated by sodium phytate.

binding energy of P 2p. From the above discussion, there exists a weak peak at 133.8 eV (Fig. 2D), corresponding to the binding energy of P 2p. From the above discussion, the MoS₂ nanosheets are successfully exfoliated from bulk MoS₂ powder in sodium phytate solution, and the phytate molecules are adsorbed onto the surface of the MoS₂ nanosheets.

3.3. Exfoliation mechanism

To investigate the effect of phytate on the exfoliation of MoS₂ nanosheets, bulk MoS₂ powder was also ultrasonically exfoliated in Na₂HPO₄ solution and ultra-pure water with the same ultrasonic time. The exfoliation yield is positively correlated with the absorption intensity of the MoS₂ nanosheets solution. As shown in Fig. S3 (ESI†), the exfoliation yield is on the order of ultra-pure water < Na₂HPO₄ solution < sodium phytate. The exfoliation yield in the Na₂HPO₄ solution is higher than that in ultra-pure water, indicating that the phosphate ion can promote the exfoliation of the MoS₂ nanosheets. The exfoliation yield in sodium phytate is higher than that in Na₂HPO₄ solution, even though the molar concentration of Na₂HPO₄ is nearly 20-folds that of sodium phytate. There are six phosphate groups in the phytate molecule, which is more efficient than Na₂HPO₄ in adsorbing on the surface of the MoS₂ nanosheets and inserting into the interlayers of bulk MoS₂, resulting in high exfoliation yield. The exfoliation process of bulk MoS₂ by sodium phytate is proposed in Scheme 1. The van der Waals force between each layer of bulk MoS₂ is destroyed by ultrasonication, and phytate molecules intercalate into the edges of the crystal interlayers to facilitate the production of MoS₂ nanosheets. After exfoliation, the adsorption of phytate on the MoS₂ nanosheets can be stably dispersed in water.

3.4. Adsorption of Hg²⁺ by MoS₂ nanosheets

The strong soft–soft interaction between Hg²⁺ and S atoms and the powerful chelation effect of phytate on the surface of the MoS₂ nanosheets inspired us to utilize MoS₂ nanosheets as adsorbents for the removal of Hg²⁺. The removal efficiency (RE)

and adsorption capacity (q_e) were calculated from eqn (1) and (2), respectively.

$$RE = \frac{(C_0 - C_e)}{C_0} \quad (1)$$

$$q_e = \frac{(C_0 - C_e) \times V}{m} \quad (2)$$

where C_0 (μg mL⁻¹) is the initial concentration of Hg²⁺, C_e (μg mL⁻¹) is the equilibrium concentration of Hg²⁺ after adsorption, q_e (mg g⁻¹) is the adsorption capacity of the MoS₂ nanosheets at equilibrium time, V (mL) is the solution volume, and m (g) is the mass of the adsorbent.

The effect of pH on the adsorption of Hg²⁺ by MoS₂ nanosheets exfoliated by sodium phytate was first investigated. As shown in Fig. S4 (ESI†), the adsorption capacity is basically unchanged over the pH range of 4.0–6.0. When the pH is higher than 6.0, the adsorption capacity is slightly decreased due to the hydrolysis of Hg²⁺. Therefore, the following adsorption experiments were conducted under acidic condition. The effect of the initial concentration of Hg²⁺ on the adsorption by MoS₂ nanosheets was investigated. As shown in Fig. 3A, the adsorption amount is gradually increased with the increasing initial concentration of Hg²⁺, and the adsorption reaches equilibrium after 1 h. However, the RE (Fig. S5, ESI†) is almost unchanged due to the low initial Hg²⁺ concentration (C_0). The adsorption kinetics was fitted by the pseudo-second-order kinetic model (3).^{11,13}

$$\frac{t}{q_t} = \frac{1}{k_2 q_e^2} + \frac{t}{q_e} \quad (3)$$

k_2 (g mg⁻¹ h⁻¹) is the pseudo-second-order adsorption rate constant, q_t (mg g⁻¹) is the adsorption amount of Hg²⁺ at time t (h), and q_e (mg g⁻¹) is the adsorption capacity at equilibrium. As shown in Fig. 3B and Table S2 (ESI†), the calculated values ($q_{e,cal}$) are close to the experimental values ($q_{e,exp}$), which indicates that the adsorption of Hg²⁺ by MoS₂ nanosheets is mainly chemical adsorption.

The adsorption thermodynamics was fitted by the Langmuir isotherm model (4).^{11,13}

$$\frac{c_e}{q_e} = \frac{1}{q_{max}} + \frac{1}{K_L q_{max}} \quad (4)$$

c_e is the equilibrium concentration (μg mL⁻¹) of Hg²⁺. q_e and q_{max} are the equilibrium adsorption capacity and the maximum

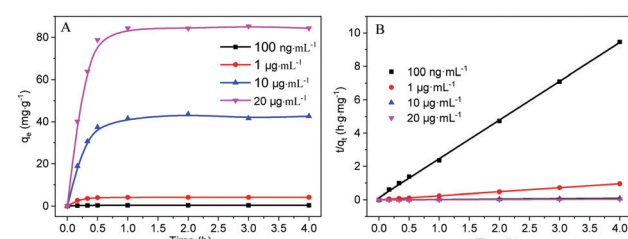


Fig. 3 (A) Adsorption of Hg²⁺ by MoS₂ nanosheets exfoliated by sodium phytate with different initial concentrations of Hg²⁺. (B) Pseudo-second-order kinetic curves for Hg²⁺ adsorption.



adsorption capacity (mg g^{-1}), respectively. K_L is the Langmuir constant. Three temperatures (25°C , 30°C , 40°C) were selected to investigate the adsorption thermodynamics. The fitting results are shown in Fig. S6 (ESI†) and listed in Table S3 (ESI†). The adsorption isotherm fitted the Langmuir model well, indicating that the adsorption of Hg^{2+} is a monolayer adsorption. The adsorption thermodynamics also indicates that the low temperature is in favor of Hg^{2+} adsorption and the highest q_{max} (313.48 mg g^{-1}) was obtained at room temperature (25°C). The Langmuir isotherm model was also used to compare the maximum adsorption capacity of MoS_2 nanosheets exfoliated by sodium phytate, and MoS_2 nanosheets exfoliated by H_2O and bulk MoS_2 powder. The results are listed in Table S4 (ESI†). The q_{max} value obtained from the MoS_2 nanosheets exfoliated by sodium phytate is about 7.5 times that of the MoS_2 powder, and about 3.7 times that of the MoS_2 nanosheets exfoliated by H_2O . This result indicates that besides the complexation of Hg^{2+} with the intrinsic S atoms of the MoS_2 nanosheets,⁴⁰ the chelating effect of phytate on the surface of the MoS_2 nanosheets plays the main role in Hg^{2+} adsorption. The interaction between the adsorbed Hg^{2+} ions and MoS_2 nanosheets exfoliated by sodium phytate were further confirmed by XPS spectrum. As shown in Fig. S7 (ESI†), a new element (Hg) appears in the survey XPS spectrum of MoS_2 nanosheets after Hg^{2+} adsorption. Furthermore, a new peak at 161.9 eV related to $\text{S } 2p_{1/2}$ of HgS is observed in the $\text{S } 2p$ core-level XPS spectrum, and the peaks at 100.9 eV and 104.9 eV are attributed to $\text{Hg}^{2+} 4f_{7/2}$ and $\text{Hg}^{2+} 4f_{5/2}$ of HgS in the $\text{Hg } 4f$ core-level XPS spectrum,⁴¹ which indicate the complex between S and Hg^{2+} . The chelating effect of phytate can be verified by the complex between O and Hg^{2+} . In the $\text{Hg } 4f$ core-level XPS spectrum, the peaks at 102.0 eV and 106.0 eV are assigned to HgO .⁴² In the $\text{O } 1s$ core-level XPS spectrum, the peaks at 530.7 eV and 532.5 eV are assigned to MoO_3 and HgO , respectively, after Hg^{2+} adsorption.⁴¹ However, without adsorption of Hg^{2+} , the peaks at 530.4 eV and 531.6 eV in the $\text{O } 1s$ core-level XPS spectrum might be deconvoluted into MoO_3 and the adsorbed water, respectively.⁴¹

The adsorption of MoS_2 nanosheets exfoliated by sodium phytate toward other heavy metal ions (Pb^{2+} , Cd^{2+} , Cr^{3+} , Mn^{2+} and Zn^{2+}) and anions (NO_2^- , NO_3^- , SO_4^{2-} and CO_3^{2-}) and their mixture with Hg^{2+} were investigated. As shown in Fig. S8 (ESI†), the MoS_2 nanosheets show a certain adsorption on Pb^{2+} and a small amount of adsorption on Cd^{2+} , Cr^{3+} , Mn^{2+} and Zn^{2+} . However, the MoS_2 nanosheets show the best adsorption on Hg^{2+} . Moreover, the co-existing heavy metal ions and anions almost do not affect the adsorption of Hg^{2+} . In the co-existence of heavy ions and anions, Hg^{2+} (100 ng mL^{-1}) still could be reduced to less than 1 ng mL^{-1} , which is the permission limit of mercury in drinking water provided by the national standard of China. These results indicate the high selectivity of MoS_2 nanosheets exfoliated by sodium phytate for Hg^{2+} adsorption due to the high affinity between Hg^{2+} and S on the surface of MoS_2 nanosheets.^{10,41}

3.5. Cell detoxification application

Before the cell detoxification experiment, MTT experiments were conducted to detect the cytotoxicity of MoS_2 nanosheets

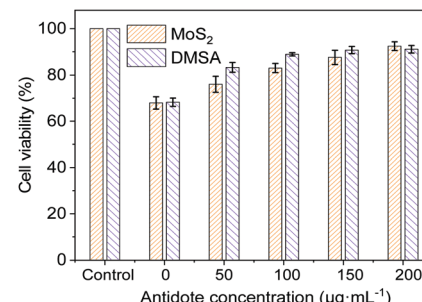


Fig. 4 Viability of HepG2 cells pre-treated with Hg^{2+} ($2 \mu\text{g mL}^{-1}$) for 2 h followed by incubation with different concentrations of MoS_2 nanosheets exfoliated by sodium phytate or DMSA for 12 h. The control was normal HepG2 cells.

exfoliated by sodium phytate, Hg^{2+} and DMSA. As shown in Fig. S9A (ESI†), the HepG2 cells maintain more than 95% cell proliferation capacity even though the concentration of the MoS_2 nanosheets is up to $250 \mu\text{g mL}^{-1}$, indicating that the MoS_2 nanosheets are highly biocompatible and have low toxicity. Hg^{2+} can induce a significant cytotoxicity in a dose-dependent manner (Fig. S9B, ESI†). Even low concentrations of Hg^{2+} can cause intoxication in HepG2 cells. $2 \mu\text{g mL}^{-1}$ and $5 \mu\text{g mL}^{-1}$ Hg^{2+} resulted in the decrease of proliferation capacities of HepG2 cells to less than 70% and 30%, respectively. In addition, DMSA showed low cytotoxicity. The proliferation capacity was more than 90% in the DMSA concentration range of $0\text{--}200 \mu\text{g mL}^{-1}$ (Fig. S9C, ESI†).

The high adsorption capacity for Hg^{2+} and low cytotoxicity of MoS_2 nanosheets inspired us to investigate their detoxification effect on Hg^{2+} poisoning. HepG2 cells were incubated with Hg^{2+} ($2 \mu\text{g mL}^{-1}$) to induce moderate cytotoxicity ($\sim 70\%$ cell viability), and then incubated with different concentrations of MoS_2 nanosheets exfoliated by sodium phytate. As shown in Fig. 4, with the increasing concentration of MoS_2 nanosheets, the proliferation capacities of HepG2 cells gradually increased. When the concentration of MoS_2 nanosheets reached $200 \mu\text{g mL}^{-1}$, the proliferation capacity of HepG2 cells was greater than 90%, which indicated that the cytotoxicity induced by Hg^{2+} was almost eliminated because the proliferation capacity of the HepG2 cells is comparable with that observed only in the presence of $200 \mu\text{g mL}^{-1}$ MoS_2 nanosheets. Compared to the detoxifier DMSA, the MoS_2 nanosheets show a similar detoxification effect, which indicates that the MoS_2 nanosheets exfoliated by sodium phytate can be used as a potential detoxifier for Hg^{2+} poisoning.

4. Conclusions

In summary, the simultaneous exfoliation and functionalization of few-layered MoS_2 nanosheets were achieved *via* ultrasonic treatment by using sodium phytate as an auxiliary reagent. The functionalization of phytate not only can facilitate the exfoliation of MoS_2 nanosheets, but also endows MoS_2 nanosheets with high stability in aqueous solution over a broad



pH range. This preparation procedure is simple, green, cost-effective, as well as high yield. The as-prepared MoS₂ nanosheets show the effective and selective adsorption for Hg²⁺ in water, and can reduce Hg²⁺ ion (100 ng mL⁻¹) to a concentration below the Chinese national permission limit of mercury (1 ng mL⁻¹) in drinking water. The as-prepared MoS₂ nanosheets also displayed low cytotoxicity for HepG2 cells, and showed a detoxification effect similar to that of the common detoxifier DMSA. The study may open a new application direction of TMDC in the development of novel therapeutics for the treatment of heavy metal poisoning.

Author contributions

Shanshan Xing: conceptualization, validation, investigation, data curation, writing – original draft; Chunqiu Xia: methodology, investigation, writing – original draft; Xinyi Liu: methodology, data curation; Liangqia Guo: conceptualization, funding acquisition, writing – review & editing, supervision; Fengfu Fu: conceptualization, writing – review & editing.

Conflicts of interest

There are no conflicts to declare.

Acknowledgements

This work was supported by the National Key Research and Development Program of China (2017YFC1600500), and the National Natural Science Foundation of China (21874023).

Notes and references

- 1 H. H. Harris, I. J. Pickering and G. N. George, *Science*, 2003, **301**, 1203.
- 2 L. Trasande, P. J. Landrigan and C. Schechter, *Environ. Health Perspect.*, 2005, **113**, 590–596.
- 3 Y. Huang, M. X. Wang, Z. J. Li, Y. Y. Gong and E. Y. Zeng, *J. Hazard. Mater.*, 2019, **373**, 783–790.
- 4 B. Manna and C. R. Raj, *ACS Sustainable Chem. Eng.*, 2018, **6**, 6175–6182.
- 5 J. P. Tang, C. J. Ptacek, D. W. Blowes, Y. Y. Liu, Y. Feng, Y. Z. Finfrock and P. Liu, *Chem. Eng. J.*, 2022, **428**, 131362.
- 6 K. Yakkala, S. Chappa, P. B. Rathod, R. N. Gurijala and A. K. Pandey, *Mater. Today Chem.*, 2021, **22**, 100507.
- 7 L. H. Dong, L. A. Hou, Z. S. Wang, P. Gu, G. Y. Chen and R. F. Jiang, *J. Hazard. Mater.*, 2018, **359**, 76–84.
- 8 L. X. Chen, Y. Wang, Y. S. Wan, Y. M. Cai, Y. Q. Xiong, Z. W. Fan, S. D. Conradson, H. Y. Fu, L. H. Yuan and W. Feng, *Chem. Eng. J.*, 2020, **387**, 124087.
- 9 X. Zhang, Z. C. Lai, C. L. Tan and H. Zhang, *Angew. Chem., Int. Ed.*, 2016, **55**, 8816–8838.
- 10 K. Ai, C. P. Ruan, M. X. Shen and L. H. Lu, *Adv. Funct. Mater.*, 2016, **26**, 5542–5549.
- 11 F. F. Jia, Q. M. Wang, J. S. Wu, Y. M. Li and S. X. Song, *ACS Sustainable Chem. Eng.*, 2017, **5**, 7410–7419.
- 12 W. Zhan, F. Jia, Y. Yuan, C. Liu, K. Sun, B. Yang and S. Song, *J. Hazard. Mater.*, 2020, **384**, 121382.
- 13 L. H. Zhi, W. Zuo, F. J. Chen and B. D. Wang, *ACS Sustainable Chem. Eng.*, 2016, **4**, 3398–3408.
- 14 Y. Song, M. Lu, B. Huang, D. Wang, G. Wang and L. Zhou, *J. Alloys Compd.*, 2018, **737**, 113–121.
- 15 P. Gao, J. Lei, J. Tan, G. Wang, H. Liu and L. Zhou, *Compos. Commun.*, 2021, **25**, 100736.
- 16 E. D. Grayfer, M. N. Kozlova and V. E. Fedorov, *Adv. Colloid Interface Sci.*, 2017, **245**, 40–61.
- 17 Z. Y. Zeng, Z. Y. Yin, X. Huang, H. Li, Q. Y. He, G. Lu, F. Boey and H. Zhang, *Angew. Chem., Int. Ed.*, 2011, **50**, 11093–11097.
- 18 A. Ambrosi, Z. Sofer and M. Pumera, *Small*, 2015, **11**, 605–612.
- 19 Y. Wang, Y. Zhou, G. Xie, J. Li, Y. Wang, X. Liu and Z. Zang, *ACS Appl. Mater. Interfaces*, 2021, **13**, 25250–25259.
- 20 D. Wang, F. Wu, Y. Song, C. Li and L. Zhou, *J. Alloys Compd.*, 2017, **728**, 1030–1036.
- 21 M. Vera-Hidalgo, E. Giovanelli, C. Navío and E. M. Pérez, *J. Am. Chem. Soc.*, 2019, **141**, 3767–3771.
- 22 A. Jawaid, D. Nepal, K. Park, M. Jespersen, A. Qualley, P. Mirau, L. F. Drummy and R. A. Vaia, *J. Am. Chem. Soc.*, 2016, **28**, 337–348.
- 23 X. Hai, K. Chang, H. Pang, M. Li, P. Li, H. M. Liu, L. Shi and J. H. Ye, *J. Am. Chem. Soc.*, 2016, **138**, 14962–14969.
- 24 S. Karunakaran, S. Pandit, B. Basu and M. De, *J. Am. Chem. Soc.*, 2018, **140**, 12634–12644.
- 25 J. F. Shen, Y. Pei, M. Wang, Y. C. Ge, P. Dong, J. H. Yuan, R. Baines, P. M. Ajayan and M. X. Ye, *Adv. Mater. Interfaces*, 2017, **4**, 1600847.
- 26 G. J. Guan, S. Y. Zhang, S. Liu, Y. Q. Cai, M. Low, C. P. Teng, I. Y. Phang, Y. Cheng, K. L. Duei, B. M. Srinivasan, Y. Zhang, Y. W. Zhang and M. Y. Han, *J. Am. Chem. Soc.*, 2015, **137**, 6152–6155.
- 27 W. Xing, Y. S. Chen, X. X. Wu, X. Z. Xu, P. Ye, T. Zhu, Q. Y. Guo, L. Q. Yang, W. W. Li and H. Huang, *Adv. Funct. Mater.*, 2017, **27**, 1701622.
- 28 N. K. Oh, H. J. Lee, K. Choi, J. Seo, U. Kim, J. Lee, Y. Choi, S. Jung, J. H. Lee, H. S. Shin and H. Park, *Chem. Mater.*, 2018, **30**, 4658–4666.
- 29 X. W. Wang and P. Y. Wu, *ACS Appl. Mater. Interfaces*, 2018, **10**, 2504–2514.
- 30 X. L. Liu, H. Chen, J. Lin, Y. Li and L. Q. Guo, *Chem. Commun.*, 2019, **55**, 2972–2975.
- 31 C. Backes, R. J. Smith, N. McEvoy, N. C. Berner, D. McCloskey, H. C. Nerl, A. O'Neill, P. J. King, T. Higgins, D. Hanlon, N. Scheuschner, J. Maultzsch, L. Houben, G. S. Duesberg, J. F. Donegan, V. Nicolosi and J. N. Coleman, *Nat. Commun.*, 2014, **5**, 4576.
- 32 C. V. Sijla Rosely, A. M. Joseph, A. Leuteritz and E. Bhoje Gowd, *ACS Sustainable Chem. Eng.*, 2020, **8**, 1868–1878.
- 33 B. Radisavljevic, A. Radenovic, J. Brivio, V. Giacometti and A. Kis, *Nat. Nanotechnol.*, 2011, **6**, 147–150.
- 34 D. D. Xuan, Y. Zhou, W. Nie and P. Chen, *Carbohydr. Polym.*, 2017, **155**, 40–48.



35 S. Park, A. T. Garcia-Esparza, H. Abroshan, B. Abraham, J. Vinson, A. Gallo, D. Nordlund, J. Park, T. R. Kim, L. Vallez, R. Alonso-Mori, D. Sokaras and X. L. Zheng, *Adv. Sci.*, 2021, **8**, 2002768.

36 H. L. Wang, P. f. Cheng, J. Shi, D. Wang, H. G. Wang, J. Pezoldt, M. Stich, R. f. Chen, A. P. A. van, W. Huang and P. Schaaf, *Green Chem.*, 2021, **23**, 3642–3648.

37 F. I. Alzakia, W. Jonhson, J. Ding and S. C. Tan, *ACS Appl. Mater. Interfaces*, 2020, **12**, 28840–28851.

38 A. A. Graf, M. J. Large, S. P. Ogilvie, Y. Rong, P. J. Lynch, G. Fratta, S. Ray, A. Shmeliakov, V. Nicolosi, R. Arenal, A. A. K. King and A. B. Dalton, *Nanoscale*, 2019, **11**, 15550–15560.

39 J. I. Paredes, J. M. Munuera, S. Villar-Rodil, L. Guardia, M. Ayán-Varela, A. Pagán, S. D. Aznar-Cervantes, J. L. Cenís, A. Martínez-Alonso and J. M. D. Tascón, *ACS Appl. Mater. Interfaces*, 2016, **8**, 27974–27986.

40 F. F. Jia, X. Zhang and S. X. Song, *Phys. Chem. Chem. Phys.*, 2017, **19**, 3837–3844.

41 R. Aswathi and K. Y. Sandhya, *J. Mater. Chem. A*, 2018, **6**, 14602.

